Optics Letters

III-V on silicon avalanche photodiodes by heteroepitaxy

Yuan Yuan,[1] Daehwan Jung,[2,3] Keye Sun,[1] Jiyuan Zheng,[1] Andrew H. Jones,[1] John E. Bowers,[2] and Joe C. Campbell[1,*]

[1]Department of Electrical and Computer Engineering, University of Virginia, Charlottesville, Virginia 22904, USA
[2]Department of Electrical and Computer Engineering, University of California Santa Barbara, Santa Barbara, California 93106, USA
[3]Center for Opto-Electronic Materials and Devices, Korea Institute of Science and Technology, Seoul 02792, South Korea
*Corresponding author: jcc7s@virginia.edu

Received 5 April 2019; revised 4 June 2019; accepted 10 June 2019; posted 17 June 2019 (Doc. ID 364252); published 11 July 2019

We demonstrate a III-V avalanche photodiode (APD) grown by heteroepitaxy on silicon. This InGaAs/InAlAs APD exhibits low dark current, gain >20, external quantum efficiency >40%, and similar low excess noise, k~0.2, as InAlAs APDs on InP.

https://doi.org/10.1364/OL.44.003538

Heterogeneous silicon photonics has drawn significant interest due to its potential for large-scale photonics integration [1]. The integration of III-V compound semiconductors with silicon photonics can reduce cost owing to economy of scale and provide high-performance III-V semiconductor devices that are compatible with Si-CMOS circuits [2]. Recently, there have been numerous reports of heterogeneous silicon photonics [3,4], such as waveguides [5], couplers, multiplexers, splitters [6], quantum dot lasers [7], distributed feedback lasers [8], ring cavities [9,10], modulators [11], and photodiodes [12,13]. However, there are no silicon photonics-compatible III-V avalanche photodiodes (APDs). III-V APDs play an important role in telecommunication systems [14], owing to their high bandwidth and high sensitivity at 1550 nm [15]. The high bandwidth enables fewer lanes in wavelength-division multiplexing or pulse amplitude modulation, which simplifies the transmission system and results in lower launch power [16]. Another potential impact area of III-V APDs is the optical interconnect, a promising approach to solve the bandwidth limitation in the post-Moore's law era. High-speed, high-efficiency, and low-cost heterogeneous silicon photonics optical interconnects have the potential to meet the tremendous data transmission demand in modern processors [17]. The high sensitivity of APDs can permit lower laser power available in optical interconnects and could improve energy efficiency by reducing the power consumption of the lasers, a key metric in future high-bandwidth-density interconnect applications, such as data centers [18]. Integrating III-V APDs with silicon photonics can also expand and improve the performance of existing applications, such as time-of-flight-based light detection and ranging (LIDAR) [19,20]. Another promising application is a next generation access network with an optical fiber to the x (FTTx) [21]. Heterogeneously integrated III-V APDs on Si can reduce cost dramatically, thereby alleviating the conflict between the data capacity and cost.

There are several approaches to integrating III-V components on silicon, such as hybrid integration and wafer bonding [10,22], but heteroepitaxial growth is the only wafer-level solution [23]. In this Letter, we report the first III-V APDs grown directly on InP/Si templates. The APD reported here is a separate absorption, charge, and multiplication (SACM) structure with an InGaAs absorber and an InAlAs multiplication region. A cross-sectional schematic of the InGaAs/InAlAs SACM APD is shown in Fig. 1(a). From top to bottom, the structure consists of a 200 nm InGaAs p-type top contact layer, a 400 nm InGaAs p-type graded-doping absorption layer, a 700 nm InGaAs unintentionally doped absorption layer, three 30 nm Al_xInGaAs grading layers, an 80 nm InAlAs charge layer, a 250 nm InAlAs unintentionally doped multiplication layer, a 65 nm InAlAs n-type layer, a 250 nm InAlAs n-type buffer layer, and a 400 nm InAlAs n-type bottom contact layer. The APD sample was grown on a 3.4 × 3.4 cm^2 InP/Si template. After 10 min of oxide desorption on the InP surface under As_2 overpressure, the growth temperature was set at 500°C, as measured by a pyrometer, for the entire APD growth. The structure of the InP/Si template is shown in Fig. 1(b) consists of a 500 nm Ge layer, 1000 nm GaAs layer, 1100 nm InAlAs linearly graded buffer layer, and 1000 nm InP layer grown by molecular beam epitaxy [13]. The InP/Si template was grown on a full 15.24 cm Si wafer without using selective area growth technique.

The mesas were formed by standard dry etching with reactive ion etch (RIE) and inductively coupled plasma (ICP). Ti/Au was deposited as the top and bottom contacts by electron-beam evaporation. After lift-off of the metals, SU-8 was spun on the sidewall as a surface passivation. Then an airbridge and GSG pads were plated. Finally, recessed windows were formed by wet etching to increase external quantum efficiency. An optical image of a 20 μm diameter InAlAs/InGaAs APD is shown in Fig. 1(c). The remaining part of the region is covered by SU-8 passivation.

The photocurrent, dark current, and gain versus bias voltage characteristics of a 20 μm diameter InGaAs/InAlAs SACM APD under 1550 nm are shown in Fig. 2. The punch-through point is approximately −14 V. The photocurrent remains flat,

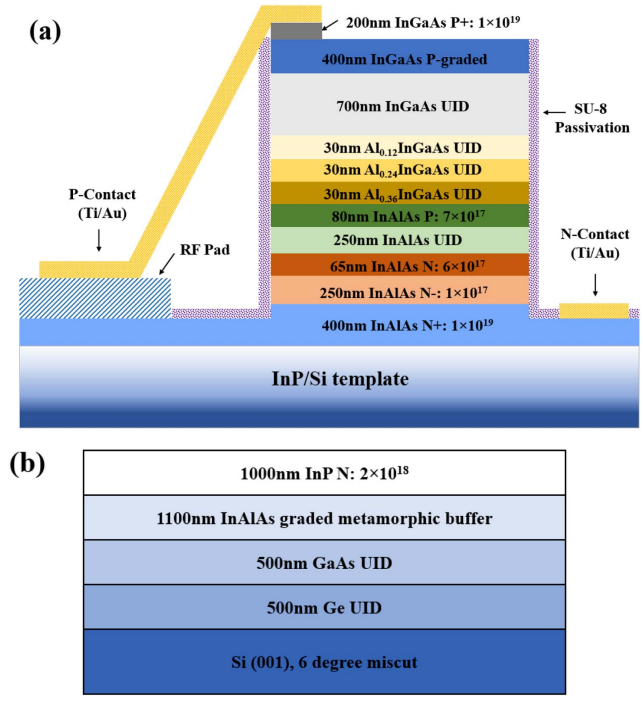

Fig. 1. (a) Schematic cross section of the InGaAs/InAlAs SACM APD on InP/Si template, (b) schematic cross section of the InP/Si template, and (c) optical image of a 20 μm diameter InGaAs/InAlAs SACM APD.

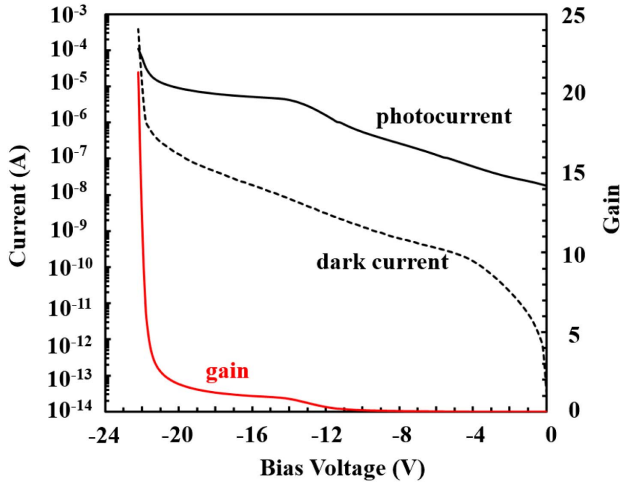

Fig. 2. Photocurrent (black solid line), dark current (black dash line), and gain (red line) versus the bias voltage of a 20 μm diameter InGaAs/InAlAs SACM APD on silicon under 1550 nm laser.

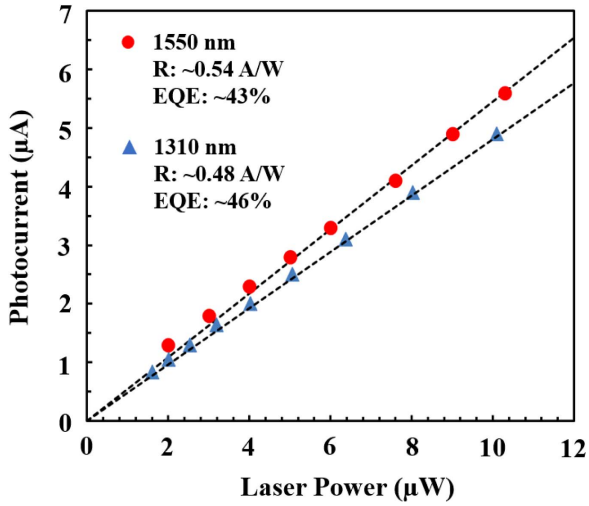

Fig. 3. Photocurrent of the InGaAs/InAlAs SACM APD on silicon versus the incident power of 1550 and 1310 nm laser.

when the bias is slightly higher than −14 V. This enables straightforward identification of the unity gain point, which was selected at −15 V. A gain >20 was achieved. Due to the three grading layers, some of the photo-generated electrons in the InGaAs absorber are injected into InAlAs multiplication layer at a low bias, which leads to a relatively high photocurrent before the punch-through point.

The circular data points in Fig. 3 show the photocurrent versus the incident power at 1550 nm (black solid circle) and 1310 nm (black solid triangle) at −15 V. These photocurrent points were measured at the unity gain point and, by linear fitting, the responsivities and the external quantum efficiencies at unity gain were calculated. For this device, the responsivity is ~0.54 and 0.48 A/W, which corresponds to an external quantum efficiency of ~43% and 46% for 1550 and 1310 nm, respectively. The absorption region is the combination of the 400 nm InGaAs *p*-type graded-doping layer and the 700 nm InGaAs unintentionally doped absorption layer. Therefore, the total absorption thickness is estimated to be ~1.1 μm.

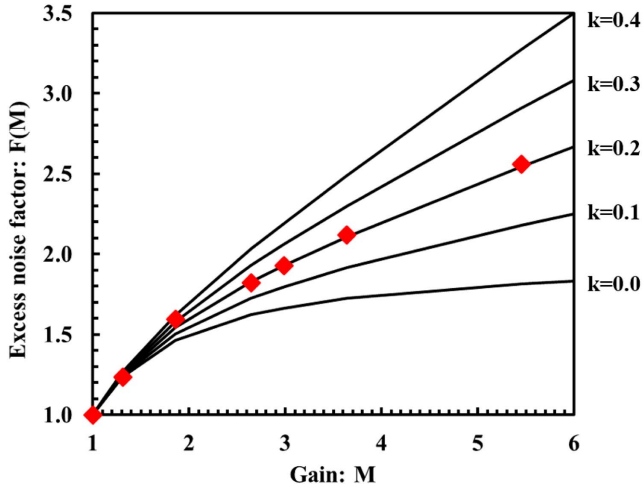

Fig. 4. Excess noise of the InGaAs/InAlAs SACM APD on silicon (red diamond) versus gian.

The absorption coefficient of InGaAs at 1550 nm is 0.82 μm^{-1} and, at 1310 nm, is 1.0 μm^{-1} [24]. If we assume that the top reflectivity without an anti-reflection coating is $R = 0.3$, it follows that the calculated external quantum efficiencies at 1550 and 1310 nm are $0.7 \times [1 - \exp(-0.82 \times 1.1)] \sim 42\%$ and $0.7 \times [1 - \exp(-1.0 \times 1.1)] \sim 46\%$, which are close to the measured results.

The excess noise characteristics were measured at 1550 nm wavelength using a noise figure meter. Since the InAlAs layers are transparent at 1550 nm, all of the photon-generated carriers are created in the two absorption layers. This results in pure electron injection into the multiplication layer, i.e., the excess noise performance will not be affected by mixed injection. The excess noise versus gain is shown in Fig. 4. The k value, which is the ratio of the hole to electron ionization coefficients, β/α, is ~0.2, which is consistent with reports on similar thickness InAlAs multiplication region APDs [25]. The InGaAs/InAlAs SACM APD grown on silicon exhibits the same excess noise as that based on InP substrate [26].

One of the primary challenges in heteroepitaxial integration is the large lattice mismatch (7.5%) and the concomitant defects in the III-V semiconductor layers, such as threading dislocations, antiphase domains, and cracks [27,28]. The issue of defects is particularly important for APDs, since they operate at a high electric field ($10^5 \sim 10^6$ V/cm). The defects can lead to a high dark current and limit the performance of APDs. In order to characterize the dark current of this APD on Si, another InGaAs/InAlAs APD on InP substrate with same epilayers was grown for comparison. The dark current densities at room temperature of both APDs are shown in Fig. 5(a). The one grown on InP has about an order of magnitude lower dark current density than the one on Si. Figures 5(b) and 5(c) illustrate the dark current from 223–323 K with a step of 20 K for the 20 μm diameter APD on Si and a 50 μm diameter APD on InP, respectively. At a low bias, both dark currents show significant temperature dependence, decreasing with temperature. However, different from the APD on InP, the temperature dependence of the APD on Si is weaker at a high bias due to trap-assisted tunneling. Unlike the generation-recombination current, the trap-assisted tunneling current is relatively independent of temperature [29].

The temperature variation of the dark current as a function of the thermal activation energy is expressed as [30]

$$I_{\text{dark}} \propto T^2 \exp\left(\frac{-E_a}{k_B T}\right), \tag{1}$$

where E_a is the activation energy, k_B is the Boltzmann constant, and T is the absolute temperature. Figure 6 shows the dark

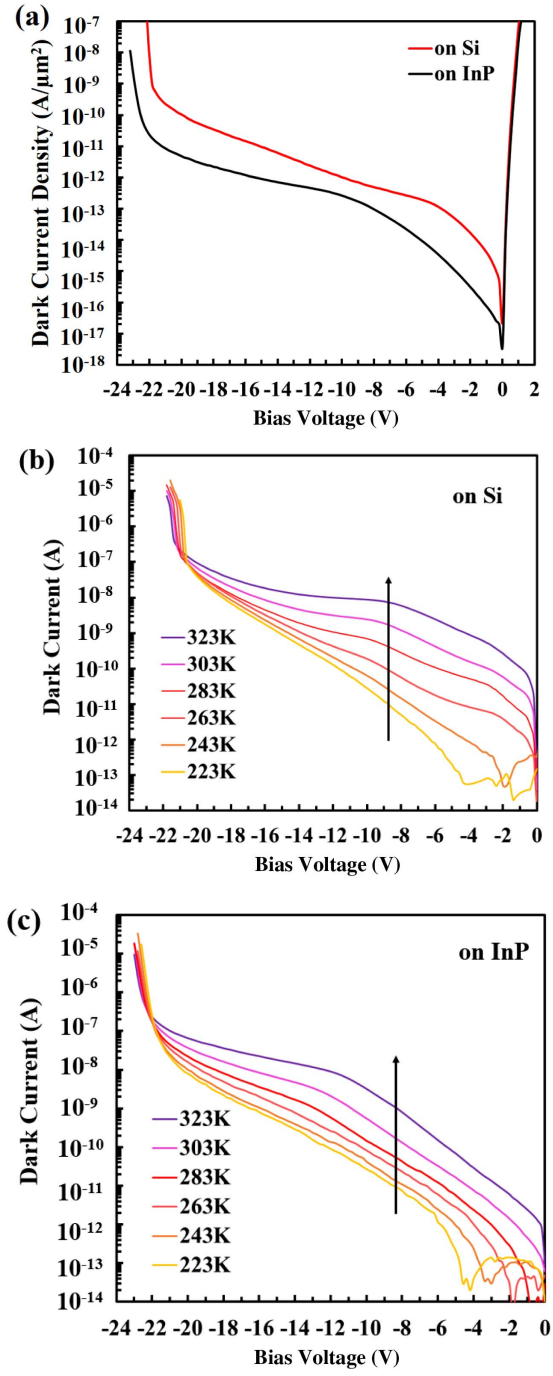

Fig. 5. (a) Dark current density at room temperature of APDs on Si and InP; temperature-dependent dark current versus the bias voltage of the (b) 20 μm diameter APD on Si and (c) 50 μm diameter APD on InP.

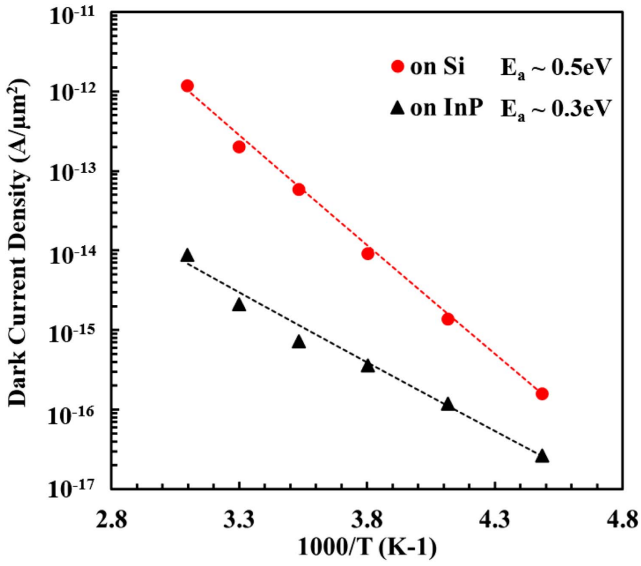

Fig. 6. Activation energies at −5 V from dark current density versus the temperature for APDs grown on Si (red solid circle) and InP (black solid triangle).

current fits using this equation at a −5 V bias, for the APDs on Si and InP, respectively. At a low bias, such as −5 V, the primary source of dark current is generation-recombination, and the activation energies are ∼0.5 and ∼0.3 eV for the APDs on Si and InP, respectively. Compared to the APD on InP, the APD on Si has a deeper generation-recombination defect center.

In conclusion, we report a III-V APD on Si with a heteroepitaxial growth method that shows a low dark current, a gain >20, external quantum efficiency >40% at communication wavelength, and similar low excess noise, $k \sim 0.2$, as InAlAs APDs on InP.

Funding. Air Force Research Laboratory (AFRL) (FA8650-15-2-5220).

REFERENCES

1. J. E. Bowers, T. Komljenovic, M. Davenport, J. Hulme, A. Y. Liu, C. T. Santis, A. Spott, S. Srinivasan, E. J. Stanton, and C. Zhang, Proc. SPIE **9774**, 977402 (2016).
2. J. E. Bowers, J. Bovington, A. Liu, and A. Gossard, in *Optical Fiber Communication Conference (OFC)* (2014), paper Th1C.1.
3. M. Seifried, G. Villares, Y. Baumgartner, H. Hahn, M. Halter, F. Horst, D. Caimi, C. Caer, M. Sousa, R. F. Dangel, L. Czornomaz, and B. J. Offrein, IEEE J. Sel. Top. Quantum Electron. **24**, 1 (2018).
4. J. E. Bowers, in *Conference on Lasers and Electro-Optics (CLEO)* (OSA, 2016), paper SM1G.1.
5. F. Xia, L. Sekaric, and Y. Vlasov, Nat. Photonics **1**, 65 (2007).
6. D. Dai and J. E. Bowers, Nanophotonics **3**, 283 (2014).
7. A. Y. Liu, R. W. Herrick, O. Ueda, P. M. Petroff, A. C. Gossard, and J. E. Bowers, IEEE J. Sel. Top. Quantum Electron. **21**, 690 (2015).
8. A. W. Fang, E. Lively, Y. H. Kuo, D. Liang, and J. E. Bowers, Opt. Express **16**, 4413 (2008).
9. P. Rabiei, J. Ma, S. Khan, J. Chiles, and S. Fathpour, Opt. Express **21**, 25573 (2013).
10. S. Srinivasan, M. Davenport, T. Komljenovic, J. Hulme, D. T. Spencer, and J. E. Bowers, IEEE Photonics J. **7**, 1 (2015).
11. L. Chen, Q. Xu, M. G. Wood, and R. M. Reano, Optica **1**, 112 (2014).
12. K. Sun, D. Jung, C. Shang, A. Liu, J. Morgan, J. Zang, Q. Li, J. Klamkin, J. E. Bowers, and A. Beling, Opt. Express **26**, 13605 (2018).
13. K. Sun, D. Jung, C. Shang, A. Liu, J. E. Bowers, and A. Beling, in *IEEE Photonics Conference (IPC)* (2017).
14. J. C. Campbell, J. Lightwave Technol. **34**, 278 (2016).
15. M. Nada, H. Yokoyama, Y. Muramoto, T. Ishibashi, and H. Matsuzaki, Opt. Express **22**, 14681 (2014).
16. M. Nada, T. Yoshimatsu, Y. Muramoto, T. Ohno, F. Nakajima, and H. Matsuzaki, in *Optical Fiber Communications Conference (OFC)* (2018), pp. 1–3.
17. M. J. R. Heck, J. F. Bauters, M. Davenport, J. K. Doylend, S. Jain, G. Kurczveil, S. Srinivasan, Y. Tang, and J. E. Bowers, IEEE J. Sel. Top. Quantum Electron. **19**, 6100117 (2013).
18. C. Zhang and J. E. Bowers, Opt. Fiber Technol. **44**, 2 (2018).
19. B. Schwarz, Nat. Photonics **4**, 429 (2010).
20. G. Adamo and A. Busacca, in *AEIT International Annual Conference (AEIT)* (IEEE, 2016).
21. A. Mitcsenkov, G. Paksy, and T. Cinkler, Photonics Netw. Commun. **21**, 253 (2011).
22. Q. Yu, Y. Wang, L. Xie, S. Nadri, K. Sun, J. Zang, Q. Li, R. M. Weikle, and A. Beling, in *Conference on Lasers and Electro-Optics (CLEO): Science and Innovations*, San Jose, California, May13 (OSA, 2018), paper SM2I-1.
23. B. Shi, Q. Li, and K. M. Lau, J. Appl. Phys. **123**, 193104 (2018).
24. S. Adachi, *Physical properties of III-V Semiconductor Compounds* (Wiley, 1992).
25. T. Nakata, J. Ishihara, K. Makita, and K. Kasahara, IEEE Photonics Tech. Lett. **21**, 1852 (2009).
26. N. Duan, S. Wang, X. G. Zheng, X. Li, N. Li, J. C. Campbell, C. Wang, and L. A. Coldren, IEEE J. Quantum Electron. **41**, 568 (2005).
27. J. C. Norman, D. Jung, Z. Zhang, Y. Wan, S. Liu, C. Shang, R. W. Herrick, W. W. Chow, A. C. Gossard, and J. E. Bowers, IEEE J. Quantum Electron. **55**, 1 (2019).
28. D. Jung, P. G. Callahan, B. Shin, K. Mukherjee, A. C. Gossard, and J. E. Bowers, J. Appl. Phys. **122**, 225703 (2017).
29. X. Li, H. Tang, T. Li, P. Wei, H. Gong, and J. Fang, Proc. SPIE **8907**, 890703 (2013).
30. Y. Yuan, A. K. Rockwell, Y. Peng, J. Zheng, S. D. March, A. H. Jones, S. R. Bank, and J. C. Campbell, IEEE J. Lightwave Technol. (to be published).